Article
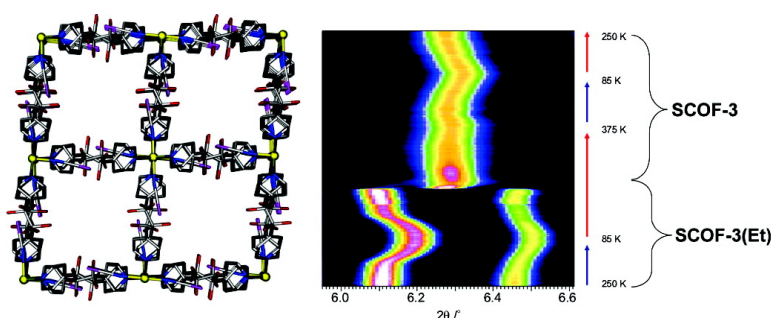
Single-Crystal to Single-Crystal Structural Transformation and Photomagnetic Properties of a Porous Iron(II) Spin-Crossover Framework

Suzanne M. Neville, Gregory J. Halder, Karena W. Chapman, Martin B. Duriska, Peter D. Southon,
John D. Cashion, Jean-Franois Ltard, Boujemaa Moubaraki, Keith S. Murray, and Cameron J. Kepert

More About This Article

Additional resources and features associated with this article are available within the HTML version:

- Supporting Information
- Links to the 4 articles that cite this article, as of the time of this article download
- Access to high resolution figures
- Links to articles and content related to this article
- Copyright permission to reproduce figures and/or text from this article

View the Full Text HTML

Single-Crystal to Single-Crystal Structural Transformation and Photomagnetic Properties of a Porous Iron(II) Spin-Crossover Framework

Suzanne M. Neville,[†,‡] Gregory J. Halder,[†,§] Karena W. Chapman,[ǁ]
Martin B. Duriska,[‡] Peter D. Southon,[†] John D. Cashion,[⊥] Jean-François Létard,[#]
Boujemaa Moubaraki,[‡] Keith S. Murray,[‡] and Cameron J. Kepert*,[†]

School of Chemistry, University of Sydney, NSW 2006, Australia, School of Chemistry, Monash University, VIC 3800, Australia, Materials Science Division, Argonne National Laboratory, Argonne, Illinois 60439, X-ray Science Division, Advanced Photon Source, Argonne National Laboratory, Argonne, Illinois 60439, School of Physics, Monash University, VIC 3800, Australia, and Laboratoire des Sciences Moléculaires, ICMCB (CNRS UPR 9048), Université Bordeaux I, 33608 Pessac, France

Received October 17, 2007; E-mail: c.kepert@chem.usyd.edu.au

Abstract: The porous coordination framework material, Fe(NCS)$_2$(bped)$_2$·3EtOH, **SCOF-3(Et)** (where bped is DL-1,2-bis(4′-pyridyl)-1,2-ethanediol), displays a spin-crossover (SCO) transition that has been stimulated both thermally and by light irradiation. The one-step thermal SCO (70−180 K) is sensitive to the presence of molecular guests, with a more gradual transition (70−225 K) apparent following the desorption of ethanol molecules that hydrogen bond to the spin centers. Additional intraframework hydrogen-bonding interactions stabilize the vacant one-dimensional pore structure of the apohost, **SCOF-3**, despite a dramatic single-crystal to single-crystal (SC−SC) structural change upon removal of the guests. Comprehensive structural analyses throughout this transformation, from primitive orthorhombic (*Pccn*) to body-centered tetragonal (*I4/mcm*), reveal a flexing of the framework and a dilation of the channels, with an accompanying subtle distortion of the iron(II) coordination geometry. Photomagnetic measurements of the light-induced excited spin state trapping (LIESST) effect have been used to assess the degree of cooperativity in this system.

Introduction

The targeted development of functional materials not only is a synthetic challenge but requires parallel characterization of structural and physical properties. At present, coordination framework materials (or metal−organic frameworks) represent an exceptionally rich field of functional materials research due in part to their structural and chemical diversity and to the potential to rationally tune their various properties.[1] Among strategic efforts to introduce specific function into these systems, the incorporation of electronic switching centers allows for the development of new advanced functional materials for molecular-scale electronic switching devices.[2−7] Spin-crossover (SCO) centers represent a convenient physically addressable molecular-

scale magnetic switch, in which $d^4−d^7$ transition metals (most commonly iron(II)) can change between the high-spin (HS) and low-spin (LS) state in response to variation in temperature, pressure, or light irradiation.[8] While SCO research has focused historically on mononuclear iron(II) species, much current attention is directed toward the coordinative-linkage of SCO sites, motivated largely by the supposition that a physical connection of this type increases cooperative communication between SCO centers toward developing bistable materials for binary switching applications.[5,8−11] Recent work has shown that

† School of Chemistry, University of Sydney.
‡ School of Chemistry, Monash University.
§ Materials Science Division, Argonne National Laboratory.
ǁ X-ray Science Division, Argonne National Laboratory.
⊥ School of Physics, Monash University.
Laboratoire des Sciences Moléculaires, Université Bordeaux I.

(1) Kepert, C. J. *Chem. Commun.* **2006**, 695−700. Kitagawa, S.; Kitaura, R.; Noro, S. *Angew. Chem., Int. Ed.* **2004**, *43*, 2334−2375. Choi, H. J.; Suh, M. P. *J. Am. Chem. Soc.* **2004**, *126*, 15844−15851. James, S. L. *Chem. Soc. Rev.* **2003**, *32*, 276−288. Eddaoudi, M.; Moler, D. B.; Li, H. L.; Chen, B. L.; Reineke, T. M.; O'Keeffe, M.; Yaghi, O. M. *Acc. Chem. Res.* **2001**, *34*, 319−330. Janiak, C. *Angew. Chem., Int. Ed.* **1997**, *36*, 1431−1434.
(2) Guionneau, P.; Marchivie, M.; Bravic, G.; Létard, J.-F.; Chasseau, D. C. *Top. Curr. Chem.* **2004**, *234*, 97−128. Real, J. A.; Andres, E.; Muñoz, M. C.; Julve, M.; Granier, T.; Bousseksou, A.; Varret, F. *Science* **1995**, *268*, 265−267.
(3) Halder, G. J.; Kepert, C. J.; Moubaraki, B.; Murray, K. S.; Cashion, J. D. *Science* **2002**, *298*, 1762−1765.
(4) Maspoch, D.; Ruiz-Molina, D.; Veciana, J. *Chem. Soc. Rev.* **2007**, *36* 770−818.
(5) Murray, K. S.; Kepert, C. J. *Top. Curr. Chem.* **2004**, *233*, 195−228.
(6) Neville, S. M.; Moubaraki, B.; Murray, K. S.; Kepert, C. J. *Angew. Chem., Int. Ed.* **2007**, *46*, 2059−2062.
(7) Shatruk, M.; Dragulescu-Andrasi, A.; Chambers, K. E.; Stoian, S. A.; Bominaar, E. L.; Achim, C.; Dunbar, K. R. *J. Am. Chem. Soc.* **2007**, *129*, 6104−6116. Vertelman, E. J.; Maccallini, E.; Gournis, D.; Rudolf, P.; Bakas, T.; Luzon, J.; Broer, R.; Pugzlys, A.; Lummen, T. T.; van Loosdrecht, P. H.; van Koningsbruggen, P. J. *Chem. Mater.* **2006**, *18*, 1951−1963.
(8) Gütlich, P.; Goodwin, H. A. *Top. Curr. Chem.* **2004**, *233*, 1−47.
(9) Bonhommeau, S.; Molnár, G.; Galet, A.; Zwick, A.; Real, J. A.; McGarvey, J. J.; Bousseksou, A. *Angew. Chem., Int. Ed.* **2005**, *44*, 4069−4073.
(10) Real, J. A.; Gaspar, A. B.; Muñoz, M. C.; Gütlich, P.; Ksenofontov, C.; Spiering, H. *Top. Curr. Chem.* **2004**, *233*, 167−193. Kahn, O.; Martinez, C. J. *Science* **1998**, *279*, 44; Létard, J.-F.; Guionneau, P.; Goux-Capes, L. *Top. Curr. Chem.* **2004**, *235*, 221−249. Hauser, A. *Top. Curr. Chem.* **2004**, *234*, 115−198.

such SCO framework materials (SCOFs) can incorporate an additional level of functionality associated with their often porous natures; guest sorption/desorption in such systems, and the associated perturbation of the iron(II) coordination environment and framework structure, provide a unique avenue for investigating the SCO phenomenon in the solid state.[3–6,9,11] For example, in [Fe(NCS)$_2$(azpy)$_2$]·1/2(guest) (where azpy is 4,4′-azopyridine), one of the few SCOFs for which the porosity has been explored,[3,6,9,11] the half SCO observed in the guest-loaded phase, is switched "off" upon removal of the guest molecules.[3] This highlights the delicate balance between the HS and LS states in SCO centers, where subtle perturbations to the host–guest system can have disproportionate effects.[3,12] Consequently, it is important to have an intimate understanding of the synergistic host–guest and magnetic properties. Moreover, novel physicochemical properties associated with these synergies are anticipated for these materials.

Here, we present the synthesis and comprehensive structural and magnetic characterization of the SCOF Fe(NCS)$_2$(bped)$_2$·3EtOH, **SCOF-3(Et)** (where bped is DL-1,2-bis(4′-pyridyl)-1,2-ethanediol), and its desolvated analogue Fe(NCS)$_2$(bped)$_2$, **SCOF-3**, using single-crystal X-ray structural analysis and magnetic susceptibility/Mössbauer spectroscopy measurements of the thermal SCO. Additionally, optical spectroscopy, magnetic susceptibility, and kinetics studies of the LIESST effect and variable-temperature single-crystal and powder X-ray diffraction methods have been used to enhance the understanding of both the magnetic properties and the structural consequences of the single-crystal to single-crystal transformation upon desolvation of this system.

Experimental Section

General Methods. All reagents were commercially available and were used as received. The ligand bped, purchased from Aldrich, was an equal mixture of *R,R* and *S,S* enantiomers (the DL form).

Synthesis of SCOF-3(Et). Solutions of bped (2 mL, 34.0 mg, 0.156 mmol) and Fe(ClO$_4$)$_2$·6H$_2$O (2 mL, 20 mg, 0.078 mmol) with NH$_4$-NCS (11.9 mg, 0.156 mmol) in ethanol were placed in separate arms of an H-shaped tube. Neat ethanol was layered above these solutions to fill the tube, which was subsequently sealed and allowed to stand. Yellow rod-shaped crystals of **SCOF-3(Et)** formed in approximately 4 weeks. The purity of this phase was confirmed by laboratory-based powder X-ray diffraction.

Single-Crystal Structural Analysis. Single-crystal diffraction data were collected for **SCOF-3(Et)** at 100 K (**SCOF-3(Et)**^{LS}) and at 200 K (**SCOF-3(Et)**^{HS}) and for **SCOF-3** at 375 K on a Bruker AXS SMART 1000 CCD diffractometer equipped with graphite-monochromated Mo Kα radiation ($\lambda = 0.7017$ Å) and an Oxford Cryosystems Cryostream. Single crystals were mounted inside open-ended 0.3 mm glass capillaries with a thin smear of grease. A single crystal of **SCOF-3(Et)** was heated at a rate of 20 K h^{-1} to 375 K to remove the solvent ethanol from the pores and single-crystal X-ray diffraction analysis carried out on the resulting apohost material, **SCOF-3**. Diffraction data analysis and reduction were performed within SMART and SAINT+.[13] Corrections for Lorentz, polarization, and absorption effects were performed within SADABS.[14] Structures were solved using a combina-

tion of direct and Patterson methods within SHELXS-97 and refined using SHELXL-97.[15] The 2-fold-disordered OH groups of the bped ligand were fixed to have 50% occupancy. All solvent accessible volumes and pore electron populations were calculated within PLATON using the VOID and SQUEEZE routines, respectively;[16] calculations of the cavity electron population for **SCOF-3** revealed no residual electron density, confirming that complete desolvation had occurred. CCDC reference numbers: CCDC-634628, -634629, and -638438.[17] Single-crystal variable-temperature unit cell collection was carried out over the range 100–375 K. The collection temperature was ramped at 20 K h^{-1} over this range during which diffraction images (3 sets of 20 images, 0.3° steps) were collected continuously using a slam-style command file within the SMART interface to follow the unit cell evolution.[13]

Powder Synchrotron X-ray Diffraction. A pulverized sample of **SCOF-3(Et)** was loaded in a polyimide capillary of 0.9 mm diameter. The sample was maintained under a continuous helium gas flow for the duration of the experiment.[18] The X-rays (20.02 keV, 0.61915 Å) available at the 1-BM beamline at the Advanced Photon Source at Argonne National Laboratory were used in combination with a MAR-345 imaging plate (IP) detector to record diffraction patterns. The sample temperature was controlled using an Oxford Cryosystems Cryostream 700 and data were collected in 1 s exposures upon continuous cooling from 250 to 85 K and then heating to 375 K, followed by cooling from 375 to 85 K, at 100 K h^{-1}. This corresponds to the collection of diffraction images at 3 K intervals. The raw images were processed using Fit-2D.[19] The sample-to-detector distance and tilt of the IP relative to the beam were refined using a LaB$_6$ standard. Le Bail analyses of the variable-temperature diffraction data were performed within GSAS.[20] Details of the refinements are included in the Supporting Information.

Thermogravimetric Analysis. Measurements on **SCOF-3(Et)** were carried out on a TA instruments Hi-Res TGA 2950 thermogravimetric analyzer. Decomposition analysis, including identification of solvent loss temperatures, was performed by heating at 0.5 K min^{-1} to 773 K; the atmosphere was controlled with a dry nitrogen supply (0.1 L min^{-1}). Ethanol vapor resolvation experiments were carried out under the same conditions with heating and cooling cycles over the range 298–373 K.

Vapor Sorption Analysis. Ethanol sorption isotherms for **SCOF-3** were measured using a Hiden-Isochema Intelligent gravimetric analyzer (IGA). A slurry of **SCOF-3(Et)** powder in ethanol was loaded into a stainless steel basket and the sample dried under high vacuum at 313 K for 24 h. An ethanol adsorption isotherm to 162 mbar was measured at 313 K using ethanol freshly distilled over magnesium turnings. At each pressure the mass of the sample was measured for 2 h, from which an equilibrium mass was extrapolated using a linear driving force model. All mass readings were corrected for buoyancy.

Magnetic Susceptibility. Magnetic susceptibility data were collected using a Quantum Design MPMS 5 SQUID magnetometer under an applied field of 1 T. The polycrystalline samples were placed in a quartz tube, and great care was taken to avoid any solvent loss and/or torquing

(11) Niel, V.; Thompson, A. L.; Muñoz, M. C.; Galet, A.; Goeta, A. S. E.; Real, J. A. *Angew. Chem., Int. Ed.* **2003**, *42*, 3760–3763.

(12) Hostettler, M.; Törnroos, K. W.; Chernyshov, D.; Vangdal, B.; Bürgi, H.-B. *Angew. Chem., Int. Ed.* **2004**, *43*, 4589–4594. Roubeau, O.; Haasnoot, J. G.; Codjovi, E.; Varret, F.; Reedijk, J. *Chem. Mater.* **2002**, *14*, 2559–2566.

(13) *SMART, SAINT and XPREP. Area detector and data integration and reduction software*; Bruker Analytical Instruments Inc.: Madison, WI, 1995.

(14) Sheldrick, G. M. *SADABS. Empirical adsorption correction program for area detector data*; University of Göttingen: Göttingen, Germany, 1996.

(15) *SHELXL97. Program for crystal structural solution and refinement*; Bruker Analytical Instruments Inc.: Madison, WI, 1997.

(16) Spek, A. L. *Platon. A multipurpose crystallography tool*; Utrecht University: Utrecht, The Netherlands, 2000.

(17) CCDC-634628, -29, and -638438 (**SCOF-3(ET)**^{HS}, **SCOF-3(ET)**^{LS}, **SCOF-3**) contain the crystal data for this paper. These data can be obtained free of charge via www.ccdc.cam.ac.uk/conts/retrieving.html {or from the Cambridge Crystallographic Data Centre, 12 Union Road, Cambridge, CB21EZ, U.K. [fax (+44)1223-336-033; deposit@ccdc.cam.ac.uk]}.

(18) Chupas, P. J.; Ciraolo, M. F.; Hanson, J. C.; Grey, C. P. *J. Am. Chem. Soc.* **2001**, *123*, 1694–1702.

(19) Hammersley, A. P. ESRF Internal Report, 1997; ESRF97HA02T. Hammersley, A. P.; Svensson, S. O.; Hanfland, M.; Fitch, A. N.; Hausermann, D. *High-Pressure Res.* **1996**, *14*, 235–248.

(20) Larson, A. C.; Dreele, R. B. V. Los Alamos National Laboratory Report LAUR 86-748, 2000.

Table 1. Crystal Data and Refinement Details for **SCOF-3(Et)**[HS], **SCOF-3(Et)**[LS], and **SCOF-3**

parameters	SCOF-3(Et)[LS]	SCOF-3(Et)[HS]	SCOF-3
spin state	LS	HS	HS
T/K	100	200	375
formula	$FeS_2C_{26}H_{24}N_6O_4 \cdot 3C_2H_6O$	$FeS_2C_{26}H_{24}N_6O_4 \cdot 3C_2H_6O$	$FeS_2C_{26}H_{24}N_6O_4$
fw	742.69	742.69	600.45
cryst system	orthorhombic	orthorhombic	tetragonal
space group	*Pccn*	*Pccn*	*I*4/*mcm*
a/Å	13.839(2)	13.875(2)	14.796(2)
b/Å	14.853(2)	15.083(2)	14.796(2)
c/Å	17.604(3)	17.970(3)	17.399(4)
V/Å^3	3618.4(10)	3760.8(9)	3808.9(11)
ρ_{calc}/Mg m^{-3}	1.363	1.312	1.047
μ/mm^{-1}	0.585	0.563	0.537
data/restraints/params	4272/0/284	4480/0/284	521/0/62
$R(F)$ [$I > 2\sigma(I)$, all]/%	7.98 [10.59]	6.24 [7.64]	8.11 [10.20]
$R_w(F^2)$ [$I > 2\sigma(I)$, all]/%	22.68 [25.43]	20.85 [23.01]	21.18 [24.39]
GoF	1.051	1.000	1.206

Table 2. Selected Structural Parameters for **SCOF-3(Et)**[HS], **SCOF-3(Et)**[LS], and **SCOF-3**

param	SCOF-3(Et)[LS]	SCOF-3(Et)[HS]	SCOF-3
intraframework hydrogen bonding	O15A⋯S1, 3.457(8); O25A⋯S1, 3.252(8); O25B⋯S1, 3.312(8)	O15A⋯S1, 3.650(6); O25A⋯S1, 3.207(5); O25B⋯S1, 3.354(6)	O1⋯S1, 3.407(14)
host−guest hydrogen bonding	O15B⋯O50, 2.866(17); O50⋯O15A, 3.671(3); O50⋯S1, 3.369(3)	O15B⋯O50, 2.765(12); O50⋯O15A, 3.293(3); O50⋯S1, 3.522(10)	
interpenetration angle/deg	85.9	85.2	90
void vol/%	29.8	31.0	34.9
dihedral angle/deg	71.6	61.9	0
N−Fe−N angle/deg	*88.82(18)−91.58(14)*	*87.78(11)−91.98(2)*	*89.5(4)−90.5(4)*
bond length (Fe−NCS)/Å	2.012(4)	2.124(3)	2.086(17)
bond length (Fe−N(py))/Å	2.096(3), 2.103(4)	2.212(2), 2.220(2)	2.177(9)

of crystallites of these potentially anisotropic HS iron(II) species, the latter avoided by dispersal of the powder in a Vaseline mull. Care was also taken to allow long thermal equilibration times at each temperature point.

Photomagnetic characterization was performed using a Kr$^+$ laser coupled through an optical fiber into the cavity of the MPMS-55 Quantum Design SQUID magnetometer operating at 2 T. Samples were prepared as a thin layer ($\sim$0.1 mg) to promote maximal penetration of the irradiated light. Solvent desorption from the material was minimized by rapid sample mounting and minimal purging of the SQUID airlock. The sample weight was obtained by comparing its thermal SCO behavior with a larger, accurately weighed sample.[21] The sample was first slow-cooled to 10 K to ensure that trapping of HS species at low temperatures did not occur. Irradiation to photosaturation was carried out a number of times using different wavelengths (i.e., 337/356.4, 406.7/415.4, 530.2, 647.1/676.4, and 752.5/799.3 nm) to determine which source was most efficient and with power intensity up to 5 mW cm^{-2}. The sample in the LS state was then irradiated with green light ($\lambda = 530.2$ nm at 5 mW cm^{-2}), the most efficient, until photosaturation was reached. Then, in the absence of irradiation, the temperature was increased at 1 K steps to 100 K to determine the T(LIESST) value and at 3 K steps over the range 100−290−10 K to follow the thermal SCO. The extreme of the $\partial\chi_M T/\partial T$ versus T plot gave the T(LIESST) value, defined as the temperature for which the light-induced HS information is erased.[21] At 10 K, the sample was again irradiated to photosaturation, and in the absence of irradiation, the relaxation kinetics at 10 K were measured for ca. 10 h.

Mössbauer Spectroscopy. Mössbauer spectra were taken using a conventional constant-acceleration drive with a symmetrical sawtooth waveform. The source of ^{57}Co in rhodium was maintained at room temperature. A fresh crystalline sample immersed in a small amount of neat ethanol, added to avoid solvent loss, was loaded into a piston type Perspex holder. The holder was placed in a coldfinger type cryostat in good thermal contact with a reservoir containing liquid nitrogen. The spectra were fitted to Lorentzian lines, with the matching lines of a doublet constrained to have the same intensity and line width.

Optical Reflectivity. Measurements were carried out using a purpose built setup in the 100−400 K temperature range. Reflectivity was investigated using a home-built reflectivity setup coupled with a SM240 spectrometer (Opton Laser International), which allows both the reflectivity spectra to be collected in the 450−950 nm range at a given temperature and the temperature dependence of the signal at a selected wavelength ($\pm$2.5 nm) between 5 and 290 K to be followed. Samples were irradiated with light over the entire temperature range of measurement. The diffuse reflected signal was calibrated using activated charcoal (Merck) as a black standard and barium sulfate (BaSO$_4$, DIN50533, Merck) as a white standard. The instrument is also equipped with an optical detector, which collects the entire reflected intensity and gives the total reflectivity signal as a function of temperature. The source of the white light consists of a halogen lamp emitting in the range 350−2400 nm. This analysis was performed directly on a thin layer of a polycrystalline sample with a small amount of liquid ethanol added to avoid desolvation but without any dispersion in a matrix.

Results

Single-Crystal X-ray Diffraction. Single-crystal refinement parameters for the HS and LS structures, **SCOF-3(Et)**[HS] and **SCOF-3(Et)**[LS], and the desolvated structure **SCOF-3** are shown in Table 1. Structural parameters of interest are included in Table 2.[22]

The material **SCOF-3(Et)** consists of interpenetrating two-dimensional (4,4) rhombic grids with Fe^{II}−*trans*-thiocyanate centers located on the vertices and bridged linearly by bped ligands (Figure 1). Parallel stacks of grids interpenetrate at an angle of 85.2° defining one-dimensional channels along the

(21) Létard, J.-F.; Guionneau, P.; Nguyen, O.; Costa, J. S.; Marcen, S.; Chastanet, G.; Marchivie, M.; Goux-Capes, L. *Chem.−Eur. J.* **2005**, *11*, 4582−4589. Létard, J.-F. *J. Mater. Chem.* **2006**, *16*, 2550−2559.
(22) We note that the "LS" structural characterization of **SCOF-3(Et)** is likely to retain a small HS fraction, since magnetic susceptibility measurements show the SCO continues with cooling below 100 K.
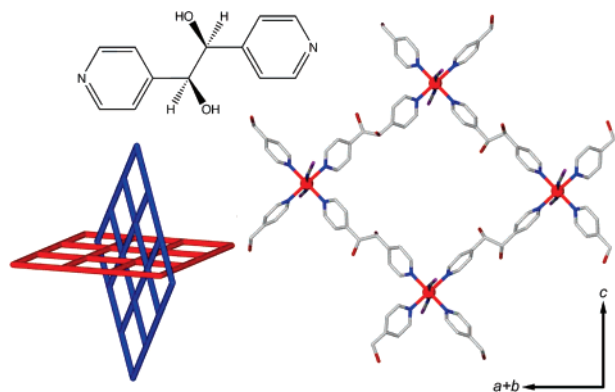
Figure 1. Representations of the DL-1,2-bis(4′-pyridyl)-1,2-ethanediol (bped) ligand, the (4,4) rhombic grid structure of **SCOF-3(Et)** omitting hydrogen atoms and guest molecules, and the network interpenetration of the rhombic grids.
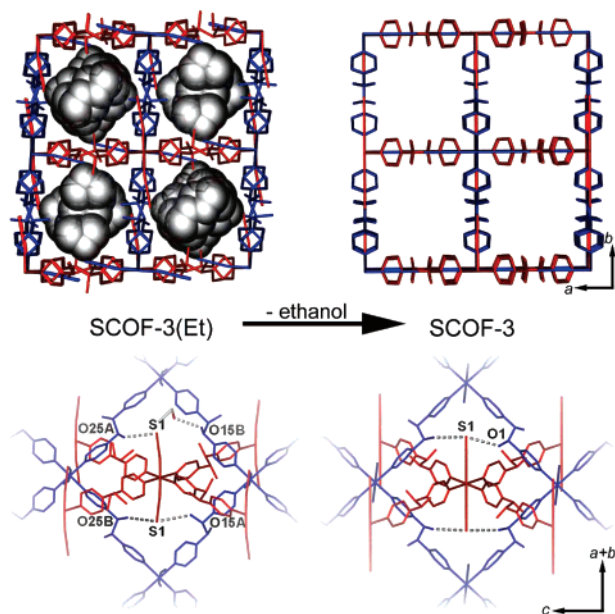
Figure 2. Representations of the single-crystal to single-crystal transformation, **SCOF-3(Et)** → **SCOF-3**, and the change in the hydrogen-bonding interactions. Some hydrogen atoms and guest molecules have been omitted.

c-axis which account for 31% of the crystal volume. The channels are undulating in shape, with cavities of dimension 8.4 × 4.7 Å separated by narrower windows of dimension 6.4 × 6.3 Å. In the as-synthesized phase two disordered ethanol molecules occupy each cavity and one disordered ethanol occupies each pore window.

Two crystallographically distinct bped ligands (*rac* form) are disordered about separate inversion centers such that their hydroxyl groups are disordered over equally occupied locations (O15A, O15B, O25A, and O25B; Figure 2) while their other atoms superimpose. No evidence was found for ordering of these units. The two bped ligands differ in the number of hydrogen-bonding interactions between the guest molecules and thiocyanate ligands within the framework structure. Of the four bped oxygen atom positions, three act as hydrogen bond donor atoms in internetwork interactions to thiocyanate acceptor sites on interpenetrating grids and the fourth forms a short hydrogen-bonding interaction with a guest ethanol molecule (Table 2). This ethanol molecule hydrogen bonds, in a significantly longer interaction, with another bped oxygen atom site and to a sulfur

atom from a thiocyanate ligand. The other two ethanol guests per formula unit, which are related by symmetry, are highly disordered and lie in the vicinity of the framework thiocyanate groups.

The overall structural topology of **SCOF-3(Et)** remains unchanged in both the HS and LS states, with the largest differences occurring in the iron(II) coordination sphere. The average Fe–N bond length, $\langle d_{Fe-N} \rangle$, and the octahedral distortion parameter, Σ, are $\langle d_{Fe-N} \rangle = 2.185$ Å, $\Sigma = 15.59°$ for **SCOF-3(Et)**[HS] and $\langle d_{Fe-N} \rangle = 2.070$ Å, $\Sigma = 10.81°$ for **SCOF-3(Et)**[LS].[23] Related variations to the framework from HS to LS include a contraction of the rhombic grids (bridged Fe–Fe distances 13.61 × 13.65 Å to 13.42 × 13.45 Å; diagonal Fe–Fe distances 17.97 × 20.49 Å to 17.60 × 20.30 Å); a slight lengthening of the bped ligands (N···N distances 9.21 and 9.23 Å to 9.25 and 9.27 Å) partially compensates for the decrease in Fe–N(bped) distances. These changes, coupled with a small increase in interpenetration angle of the two-dimensional rhombic grids (85.2 to 85.9°), lead to subtle changes to the channel dimensions (cavities 8.4 × 4.7 Å to 8.2 × 4.8 Å; windows 6.4 × 6.3 Å to 6.7 × 6.3 Å) and a reduction in calculated accessible void volume (31.0 to 29.8%). The internetwork and host–guest hydrogen bonding interactions found in **SCOF-3(Et)**[HS] are retained in the LS state with some variation in relative distances (Table 2).

The general framework topology is maintained following the single-crystal to single-crystal structural transition from **SCOF-3(Et)** to **SCOF-3**. However, dramatic framework flexibility is observed. The most significant structural change is an increase in the interpenetration angle of the two-dimensional grids from 85.2 to 90°, with the symmetry increasing from primitive orthorhombic (*Pccn*) to body-centered tetragonal (*I4/mcm*). There is a concomitant increase in accessible void volume from 31.0% to 34.9% associated with a dilation of the cavities (6.8 × 6.8 Å) and contraction of the pore windows (5.2 × 5.2 Å). The intraframework interactions are retained following desolvation, and an additional intraframework (hydroxyl to thiocyanate) hydrogen bond (O1···S1: 3.407(14) Å) is formed such that both OH groups of the now structurally equivalent bped ligands participate in intraframework contacts.

Significant changes to the iron(II) geometry occur with framework desolvation. The octahedral distortion of the iron-(II) center decreases from $\Sigma = 15.6°$ for **SCOF-3(Et)**[HS] to $\Sigma = 2.0°$ for **SCOF-3**.[23] There is a concomitant straightening of the bound thiocyanate units (FeNC(S) = 168.5(3) to 180°) and a rotation of the pyridyl donors about the iron(II) center (dihedral angle = 61.9 to 0°). The average Fe–N bond length $\langle d_{Fe-N} \rangle = 2.14$ Å at 375 K is consistent with iron(II) in the HS state and is noticeably shorter than for **SCOF-3(Et)**[HS], despite the higher temperature of measurement.

Thermogravimetric Analysis. Thermogravimetric analysis of **SCOF-3(Et)** indicated that the ethanol guest is removed from the pores with heating to ca. 325 K. The desolvated material **SCOF-3** is stable up to 400 K above which thermal decomposition occurs.

Vapor Sorption Analysis. The apohost framework **SCOF-3** achieves a 13 wt % sorption of ethanol vapor at low partial

(23) Guionneau, P.; Brigouleix, C.; Barrans, Y.; Goeta, A. E.; Létard, J.-F.; Howard, J. A.; Gaultier, J.; Chasseau, D. C. *R. Acad. Sci., Ser. 2c* **2001**, *4*, 161–171.
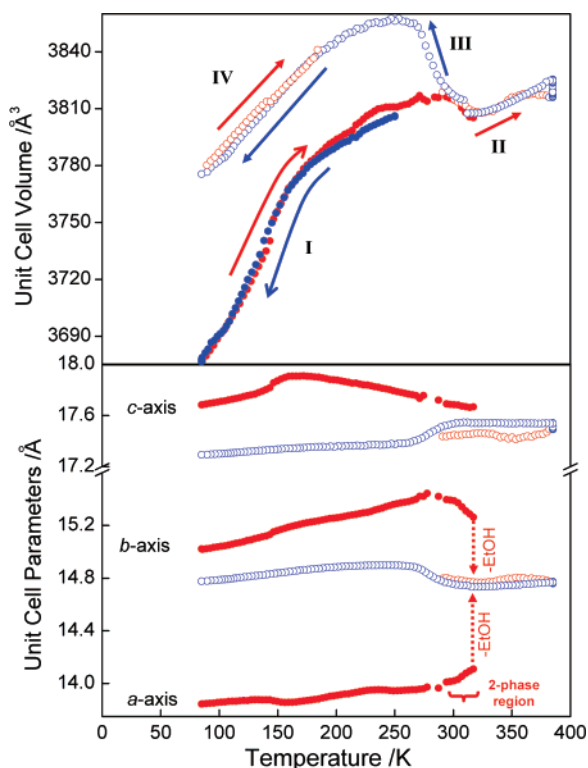
Figure 3. Evolution of the unit cell volume (above) and lattice parameters (below) from powder X-ray diffraction data indicating (I) SCO of **SCOF-3(Et)**, 250−85−250 K (●), (II) desolvation 250−375 K, (III) cooling of **SCOF-3**, 375−250 K, and (IV) SCO of **SCOF-3**, 250−85−250 K (○). Data obtained with heating and cooling are shown in red and blue, respectively.

pressures ($P/P_0 = 0.4$), corresponding to a ca. 60% resorption. Application of higher partial pressures gave a further small uptake to a maximum of 16 wt %, corresponding to ca. 70% resorption. The rate of ethanol sorption was comparatively slow over all pressures, with many of the points below $P/P_0 = 0.4$ still approaching equilibrium after 2 h. This suggests that kinetic trapping of the ethanol guests occurs in the narrow pore windows and/or at defect sites within the 1D channels. Considerable hysteresis was observed between the adsorption and desorption arms of the isotherm at low pressures, suggestive of energy differences associated with framework structural change.

Variable-Temperature Single-Crystal X-ray Diffraction Analysis. The temperature dependence of the lattice parameters of a single-crystal sample of **SCOF-3(Et)** was followed over the range 100−375 K, which encompasses the thermal SCO of **SCOF-3(Et)** through to the desolvated material **SCOF-3**. Over the range 100−180 K the lattice parameters show features parallel to those of the temperature-dependent magnetic susceptibility, reflecting the expansion of Fe−N bond lengths with the SCO.[6] At 325 K there are dramatic changes observed in the lattice parameters, where a phase transition occurs from orthorhombic to tetragonal symmetry. The most notable changes occur over the *a*- and *b*-axes (ca. 5%) as the independent orthorhombic parameters, *a* and *b*, converge to a single tetragonal parameter.

Variable-Temperature Powder X-ray Diffraction Analysis. The temperature dependence of the lattice parameters from variable-temperature synchrotron powder X-ray diffraction (Figure 3) shows four distinct regions of interest: SCO of
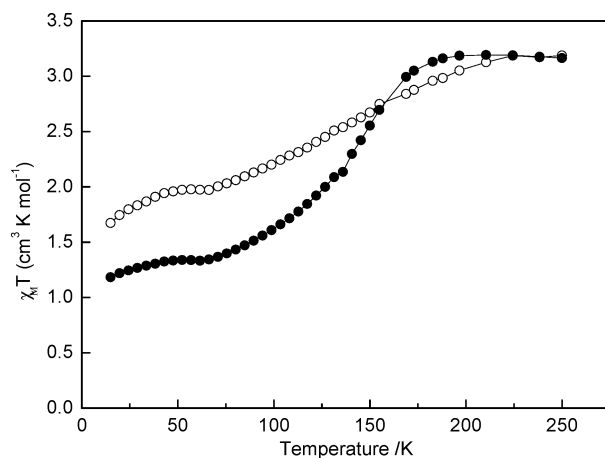
Figure 4. Plot of $\chi_M T$ versus temperature for **SCOF-3(Et)** (●) and **SCOF-3** (○).

SCOF-3(Et); crystal transformation process **SCOF-3(Et)** → **SCOF-3**; apohost **SCOF-3**; SCO of **SCOF-3**.

(a) SCO of SCOF-3(Et). On cooling of the sample from 250 to 180 K, the *a*- and *b*-axes contract steadily and the *c*-axis expands. With cooling through the onset of the SCO transition from 180 to 135 K, the unit cell axes undergo pronounced, continuous changes, with the *a* parameter increasing and *b* and *c* decreasing. With continued cooling through the transition from 135 to 85 K, each of the *a*−*c* parameters decreases gradually. The unit cell volume shows a gradual decrease over the entire range 250−85 K, with a 3.5% overall change. On heating of the sample back to 250 K, no thermal hysteresis in lattice parameters is evident. The data in the region 250−85−250 K and with further heating to 298 K were fit in the orthorhombic space group *Pccn*.

(b) Crystal Transformation Process SCOF-3(Et) → SCOF-3. The data in this region were fit with a two phase Le Bail refinement of the orthorhombic and tetragonal space groups *Pccn* and *I4/mcm*, respectively, with the gradual decrease in the fraction of the orthorhombic phase and a concurrent increase in the fraction of the tetragonal phase. Over this range, for the orthorhombic phase parameters, the *a*-axis increases gradually and the *b*- and *c*-axes and unit cell volume decrease gradually. As observed by single-crystal diffraction, at the phase transition the two orthorhombic parameters converge to a single tetragonal parameter with a dramatic increase and associated decrease in the *a*- and *b*-parameters, respectively. Above 325 K, the phase transition is complete, and with further heating to 375 K, the lattice parameters undergo uniform positive thermal expansion. These and the remaining data were fit in the tetragonal space group *I4/mcm*.

(c) Apohost SCOF-3. The *a*- and *c*-axes and unit cell volume decrease slightly over the range 375−310 K due to thermal contraction. However, between 310 and 250 K a rapid increase in the *a*-axis and unit cell volume and a decrease in the *c*-axis is observed.

(d) SCO of SCOF-3. Over the entire range the *a*- and *c*-axes and the unit cell volume decrease steadily with a 2.1% overall change. No thermal hysteresis is evident.

Temperature-Dependent Magnetic Susceptibility. Magnetic susceptibility studies were used to follow the iron(II) spin state changes for a polycrystalline sample of **SCOF-3(Et)** from 15 to 250 K (Figure 4). The $\chi_M T$ values for **SCOF-3(Et)**
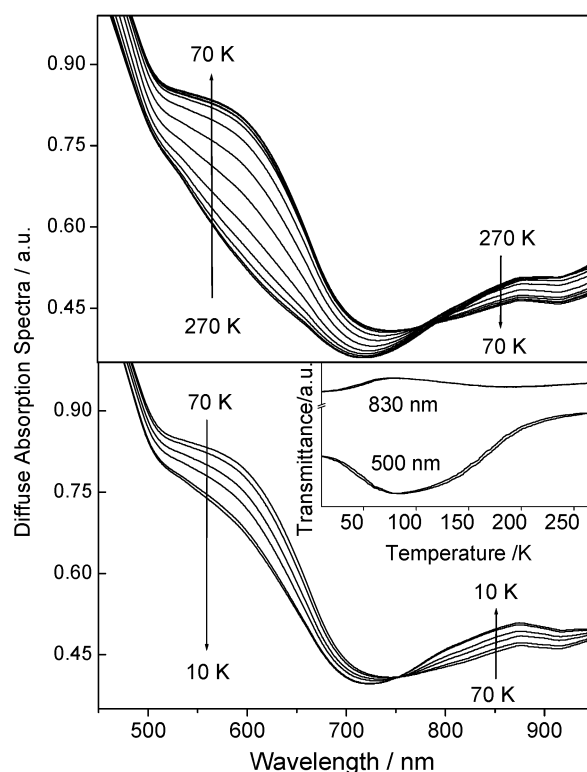
remained approximately constant at ca. 3.2 cm^3 K mol^{-1} between 280 and 180 K, which is in the range of values expected for HS iron(II). Below 180 K, $\chi_M T$ initially decreased rapidly and then proceeded more gradually, reaching a minimum value of ca. 1.2 cm^3 K mol^{-1} below 70 K suggesting an incomplete SCO with a residual HS fraction at low temperatures of ca. 0.37. The $T_{1/2}$ value is 137 K (calculated as the temperature at which half of the iron(II) centers which are observed to crossover are in the HS state). On quench-cooling, a small amount of HS trapping was observed below 70 K.

Magnetic susceptibility measurements of **SCOF-3** revealed a more gradual SCO over a wider temperature range (225–70 K) with residual HS fraction to ca. 0.53, an increase of 16% compared to **SCOF-3(Et)**. The $T_{1/2}$ value for **SCOF-3** is decreased to ca. 125 K, compared to 137 K for **SCOF-3(Et)**. No hysteresis was observed in the $\chi_M T$ values for either **SCOF-3(Et)** or **SCOF-3**.

Mössbauer Effect. The Mössbauer spectrum (see Supporting Information) recorded at 82 K for **SCOF-3(Et)** was best fitted as three quadrupole doublets due to coexisting LS sites (δ = 0.49 mm s^{-1}, ΔE_Q = 0.06 mm s^{-1}) and two HS sites (δ = 1.16 mm s^{-1}, ΔE_Q = 0.63 mm s^{-1}; δ = 1.16 mm s^{-1}, ΔE_Q = 1.00 mm s^{-1}). The LS:HS:HS area ratio is 43:11:46, which is different from the ca. 55:45 LS:HS ratio expected from the susceptibility data for **SCOF-3(Et)** and approaching the ca. 34: 66 ratio expected from the susceptibility data for **SCOF-3**. Such a discrepancy is not unexpected in view of differing Debye Waller factors for the two spin states, although it may also arise from a partial desolvation of the sample prior to measurement.[24]

Optical Reflectivity. Figure 5 illustrates the spectral changes for **SCOF-3(Et)** with temperature (10–270–10 K) and wavelength (450–950 nm). Between 270 and 70 K the band at 550 nm increased and the band at 850 nm decreased. Between 70 and 10 K the band at 550 nm decreased and the band at 850 nm increased, suggesting some LIESST of HS sites. The temperature dependence of the relative transmittance at the wavelengths 500 and 830 nm was followed for **SCOF-3(Et)** (Figure 5, inset). The band at 500 nm shows a gradual decrease between 270 and 70 K followed by an increase to 10 K of approximately one-third of the intensity as the signal measured at 270 K. The band at 830 nm shows the inverse of that at 500 nm. With repeated heating and cooling over the range 10–70 K (the region of the LIESST), no light-induced thermal hysteresis (LITH) effect[21] was observed.

Light-Induced Magnetic Susceptibility. The direct magnetic consequences of irradiation to a thin layer of **SCOF-3(Et)**, by irradiating the $^1A_1 \rightarrow {}^1T$ absorption band with green light (λ = 530.2 nm), was carried out by SQUID magnetometry with irradiation at 10 K (Figure 6). The $\chi_M T$ values at 10 K attained a maximum value of 1.78 cm^3 K mol^{-1}, indicating an incomplete photoexcitation of ca. 30%, consistent with that observed at the surface by optical reflectivity. Without irradiation, the magnetic response between 10 and 25 K appears to be temperature independent as there is an observed increase in $\chi_M T$ over this range, to a maximum of 1.85 cm^3 K mol^{-1}. This increase in $\chi_M T$ reflects that seen over the same temperature range in the thermal SCO (Figure 4) and is attributed to zero-field splitting

(24) Desaix, A.; Roubeau, O.; Jeftic, J.; Haasnoot, J. G.; Boukheddaden, K.; Codjovi, E.; Linares, J.; Nogues, M.; Varret, F. *Eur. Phys. J. B* **1998**, *6*, 183–193.

Figure 5. Diffuse absorption spectra of **SCOF-3(Et)** over 70–270 K for the thermal SCO (above) and 70–10 K (below) for the LIESST effect. The transmittance versus temperature at 500 and 830 nm, related to the d–d and MLCT changes, is inset.
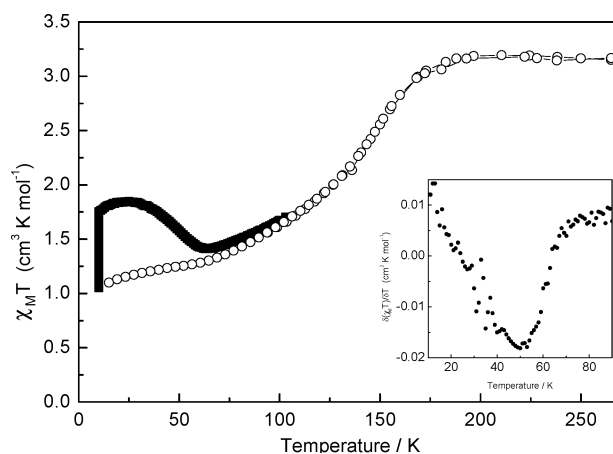
Figure 6. $\chi_M T$ versus temperature over the range 10–275 K for the photomagnetic effect for **SCOF-3(Et)** (■, irradiation at 530.2 nm followed by relaxation; ○, thermal SCO). Inset: Plot of $\delta\chi_M T/\delta T$ versus temperature indicating a T(LIESST) value of 55 K at the minimum.

of the HS iron(II) metal centers. Notably, over the range 10–70 K, without irradiation, the material does not relax completely to the minimum attained at 10 K (minimum $\chi_M T$ value of 1.7 cm^3 K mol^{-1}), suggesting a competition between photoinduced excitation and relaxation times. The relaxation kinetics after photosaturation were followed at 10 K and display a rapid initial component followed by a very long decay process,[25] where only a ca. 40% relaxation of the metastable HS state to the LS state was observed after 24 h. The T(LIESST) value is defined as the minimum of the $\delta\chi_M T/\delta T$ versus T curve[21] for which the material has been heated at a defined rate for all samples, in

the absence of irradiation the material; here, **SCOF-3(Et)** has a T(LIESST) value of 55 K (Figure 6, inset).

It is instructive to position **SCOF-3(Et)** within the classification scheme of iron(II) SCO systems compiled by one of us that classifies iron(II) SCO systems according to their $T_{1/2}$ and T(LIESST) values.[21] This database demonstrates a trend where materials can be classified on the basis of the geometry and rigidity of the ligands around the iron(II) center and, in turn, the degree of cooperativity between the SCO sites. The relationship between the two parameters is a maximum line defined by T(LIESST) $= T_0 - 0.3T_{1/2}$ where, to date, four T_0 values have been identified and reported: $T_0 = 100$ K for unidentate ligands,[26] 120 K for bidentate ligands,[26] 150 K for meridional tridentate ligands,[27] and 200 K for three-dimensional network solids.[28] The T(LIESST) and $T_{1/2}$ values of 55 and 137 K, respectively, place this phase in the $T_0 = 100$ K family, representing the upper limit for unidentate ligands.[21]

Discussion

Although the general SCO features are retained in the transition from **SCOF-3(Et)** to **SCOF-3**, changes in the structure—specifically the framework transformation and additional hydrogen bond formation—produce clear differences in SCO behavior. This highlights the delicate balance between HS and LS states in SCO systems. There is a stabilization of the LS state, evidenced from a ca. 45 K increase in the onset of SCO, which is consistent with the observed decrease in distortion of the iron(II) coordination environment. In contrast, in the SCOF [Fe(NCS)$_2$(azpy)$_2$]·1/2(guest) and typical mononuclear iron(II) systems, the loss of intermolecular interactions stabilizes the HS state, often eliminating the SCO behavior.[3,8,11] In this study, and in limited other systems,[6,12,29] the general retention of intramolecular interactions upon guest removal contributes to the stabilization of the LS state.

In addition to the increase in SCO temperature in **SCOF-3**, the spin transition is noticeably broadened, resulting in a greater residual HS fraction at low temperature. As the single-crystal and powder diffraction studies confirm the retention of sample crystallinity throughout the transition, a change in sample condition can be discounted as a basis for the broader SCO. Instead, this fundamental effect is likely to reflect a greater distribution of local magnetic iron(II) environments, as is consistent with the mixture of multiple LS and HS sites in the Mössbauer spectrum.[30]

The inclusion of the bped ligand, functionalized with hydroxyl groups, contributes to the structural rearrangement upon desolvation driven by the rearrangement of hydrogen-bonding interactions to form additional intraframework interactions. As such, the motivation for the observed single-crystal to single-crystal transformation can be attributed to the dynamic interplay

of these host—guest and intraframework interactions. Few examples of crystal transformations involving such pronounced structural changes exist,[31,32] with perhaps the most closely related case being with the dehydration of the hydrogen-bonded clathrate [Co(H$_2$O)$_6$]H$_2$(TC-TTF)·2H$_2$O, in which one host—guest and five host—host hydrogen-bonding interactions convert to six host—host interactions.[32] In the topologically related SCOF [Fe(NCS)$_2$(bpbd)$_2$]·acetone, which exclusively contains intraframework interactions, no hydrogen bonds are broken/formed upon desolvation, resulting in an inflexible phase.[6] The structure-stabilizing role of the intraframework hydrogen-bonding interactions in the present system is further evident from the 4% relative increase in accessible void volume in **SCOF-3**. This is contrary to generic expectations on the basis of space-filling considerations, where a reduction in pore volume to maximize intraframework contacts may be anticipated, with the extreme case being a collapse of framework structure. Despite the increased void volume, attempts to resorb ethanol vapor into **SCOF-3** resulted in incomplete uptake compared to the as-synthesized phase **SCOF-3(Et)**. This suggests that the reverse **SCOF-3** → **SCOF-3(Et)** structural transformation is not readily achievable, due possibly to a significant activation barrier to breaking the additional intraframework hydrogen bonds. The reduced ethanol uptake may be attributed to the different shape (curvature) and surface chemistry (now hydrophobic) of the pores of **SCOF-3**.

In addition to the general framework flexibility, the bped ligands linking the iron(II) SCO centers display an inherent elasticity through the SCO transition. These bridges appear to confer little communicative influence, steric and/or electronic, to the thermal and photoexcitation properties of **SCOF-3(Et)**, as seen in the gradual thermal transition, the partial excitation and stretched-exponential decay of the photoexcited state with slow relaxation, and the absence of LITH.[21] In further support of this, the T(LIESST) value of 55 K places the material below the $T_0 = 100$ K line for monodentate discrete materials.[33] We postulate that the coordinative bridging of iron(II) centers with elastic ligands, such as bped, may have a negative relative influence on cooperativity, in direct contrast to the positive influence observed with short rigid ligands.[7,11,34]

Conclusions

We report porous SCOF materials, **SCOF-3(Et)** and **SCOF-3**, with unique guest-dependent structural and SCO properties. The material **SCOF-3(Et)** is novel among SCOFs in containing both intraframework and host—guest hydrogen-bonding interactions, each playing pivotal roles in directing the flexible single-crystal to single-crystal transformation and solvent-sensitive

(25) Decurtins, S.; Gütlich, P.; Hasselbach, K. M.; Hauser, A.; Spiering, H. *Inorg. Chem.* **1985**, *24*, 2174—2178.

(26) Létard, J.-F.; Capes, L.; Chastanet, G.; Moliner, N.; Létard, S.; Real, J. A.; Kahn, O. *Chem. Phys. Lett.* **1999**, *313*, 115—120.

(27) Carbonera, C.; Costa, J. S.; Money, V. A.; Elhaik, J.; Howard, J. A. K.; Halcrow, M. A.; Létard, J.-F. *Dalton Trans.* **2006**, 3058—3066. Money, V. A.; Costa, J. S.; Marcén, S.; Chastanet, G.; Elhaik, J.; Halcrow, M. A.; Howard, J. A. K.; Létard, J.-F. *Chem. Phys. Lett.* **2004**, *391*, 273—277. Marcén, S.; Lecren, L.; Capes, L.; Goodwin, H. A.; Létard, J.-F. *Chem. Phys. Lett.* **2002**, *358*, 87—95.

(28) Shimamoto, N.; Ohkoshi, S.-S.; Sato, O.; Hashimoto, K. *Inorg. Chem.* **2002**, *45*, 678—684.

(29) Amoore, J. J.; Kepert, C. J.; Cashion, J. D.; Moubaraki, B.; Neville, S. M.; Murray, K. S. *Chem.—Eur. J.* **2006**, *12*, 8220—8227.

(30) Hauser, A.; Adler, J.; Gütlich, P. *Chem. Phys. Lett.* **1988**, *152*, 468—472.

(31) Halder, G. J.; Kepert, C. J. *Aust. J. Chem.* **2006**, *59*, 597—604. Lin, X.; Blake, A. J.; Wilson, C.; Sun, X. Z.; Champness, N. R.; George, M. W.; Hubberstey, P.; Mokaya, R.; Schröder, M. *J. Am. Chem. Soc.* **2006**, *128*, 10745—10753. Suh, M. P.; Cheon, Y. E. *Aust. J. Chem.* **2006**, *59*, 605—612. Kitagawa, S.; Uemura, K. *Chem. Soc. Rev.* **2005**, *34*, 109—119. Kurmoo, M.; Kumagai, H.; Chapman, K. W.; Kepert, C. J. *Chem. Commun.* **2005**, 3012—3014. Kitaura, R.; Fujimoto, K.; Noro, S.; Kondo, M.; Kitagawa, S. *Angew. Chem., Int. Ed.* **2002**, *41*, 133—135. Fletcher, A. J.; Cussen, E. J.; Prior, T. J.; Rosseinsky, M. J.; Kepert, C. J.; Thomas, K. M. *J. Am. Chem. Soc.* **2001**, *123*, 10001—10011.

(32) Kepert, C. J.; Hesek, D.; Beer, P. D.; Rosseinsky, M. J. *Angew. Chem., Int. Ed.* **1998**, *37*, 3158—3160.

(33) Leita, B. A.; Neville, S. M.; Halder, G. J.; Moubaraki, B.; Kepert, C. J.; Létard, J.-F.; Murray, K. S. *Inorg. Chem.* **2007**, *46*, 8784—8795. Absmeier, A.; Bartel, M.; Carbonera, C.; Jameson, G. N.; Caneschi, A.; Mereiter, K.; Létard, J.-F.; Linert, W. *Chem.—Eur. J.* **2006**, *12*, 2235—2243.

(34) Niel, V.; Martinez-Agudo, J. M.; Muñoz, M. C.; Gaspar, A. B.; Real, J. A. *Inorg. Chem.* **2001**, *40*, 3838—3839.

SCO behavior. In situ variable-temperature single-crystal and powder X-ray diffraction—techniques rarely utilized for such systems—have provided a comprehensive insight into both the magnetic and structural consequences of the transformation. The unusual LS stabilization following desolvation from **SCOF-3(Et)** to **SCOF-3** is unique for a flexible SCOF material and highlights the tunability of SCO transitions through relatively small structural changes.

We aim in the future to explore the influence of a range of guest molecules, in particular those with the ability to form direct hydrogen-bonded linkages between SCO centers, on the degree of cooperativity between crossover sites in this interpenetrated lattice; such an approach promises significant new insight into structure—property relationships in SCO systems. Further, the unique observation of light-induced SCO in this porous framework points to the possibility of stimulating host—guest processes by light irradiation; partial bleaching to the LS state at ambient temperature is anticipated, for example, to provide a novel mechanism for the controlled release or uptake of guest species.

Supporting Information Available: Details of in-situ single-crystal X-ray diffraction, thermogravimetric analysis, vapor isotherms, powder diffraction analysis, and Mössbauer spectroscopy and tables of χ^2 values and photomagnetism kinetics studies. This material is available free of charge via the Internet at http://pubs.acs.org.

JA077958F